行政院國家科學委員會專題研究計畫 成果報告

抗癌試劑 2-苯乙烯色素母酮、噢哢及氧二苯甲酮衍生物之藥物設計及合成(第 2 年)
研究成果報告(完整版)

計 畫 類 別 ：個別型
計 畫 編 號 ：NSC 96-2113-M-032-007-MY2
執 行 期 間 ：97 年 08 月 01 日至 98 年 07 月 31 日
執 行 單 位 ：淡江大學化學系

計 畫 主 持 人 ：蕭永政

處 理 方 式 ：本計畫可公開查詢

中 華 民 國 98 年 12 月 25 日

3,5-Diaryl-*1H*-pyrazole as a molecular scaffold for the synthesis of apoptosis-inducing agents

Arthur Y. Shaw,[a,*] Hao-Han Liau,[a] Pei-Jung Lu,[b] Chien-Hsing Lee,[b] Chia-Ning Yang,[c] Jun-Yan Chen[d]

[a] Department of Chemistry, Tamkang University, Taipei 251, Taiwan.

[b] Institute of Clinical Medicine, National Cheng Kung University, Tainan 701, Taiwan.

[c] Institute of Biotechnology, National University of Kaohsiung, Kaohsiung 700, Taiwan.

[d] Department of Life Science, National University of Kaohsiung, Kaohsiung 700, Taiwan.

[*]To whom correspondence should be addressed: Tel.: 886-2-2621-5656 ext.2842; fax: 886-2-2620-9924. E-mail address: shaw.299@gmail.com (A. Y. Shaw).

Keywords: 3,5-diaryl-*1H*-pyrazole, molecular scaffold, apoptosis-inducing agent, mitochondrial apoptotic pathway, structure-activity relationship.

Abstract

A series of 3,5-diaryl-*1H*-pyrazole analogs were synthesized and evaluated for their growth-inhibitory effect on carcinoma cells. Our findings suggested that analogs bearing electron-withdrawing groups on one ring while electron-donating groups on another exhibited significant activity. Moreover, **26** bearing a 1,1'-biphenyl moiety displayed the most potent activity against OVCA, SW620, H460 and AGS cells with GI_{50} values of 0.67, 0.89, 0.73 and 0.79 μM, respectively. The mechanistic study demonstrated that **26**- and **27**-induced growth inhibition in OVCA cells might be, in part, attributed to the inhibition of Akt activity, following by the mitochondrial apoptotic pathway evidenced by the activation of caspase-9, caspase-3, and the cleavage of protein poly(ADP-ribose) polymerase (PARP) and DNA fragmentation. The structure-activity relationship study was further carried out by Comparative Molecular Field Analysis (CoMFA) with q^2 and R^2 values of 0.671 and 0.846, respectively, indicating its predictivity and accountability for future study.

1. Introduction

Apoptosis, or programmed cell death, is the prevalent mechanism for cellular development and differentiation. Deregulation of apoptosis is widely believed to be involved in a variety of human diseases, including cancer, autoimmune diseases, and neurodegeneration disorders.[1,2] Appreciable progress in elucidating molecular components of the apoptotic machinery have resulted in the identification of many molecular targets for the development of new dugs with pro- and anti-apoptotic activity to treat different diseases including cancer. So far, two principle apoptotic pathways are identified, the death receptor (or extrinsic) and the mitochondria (or intrinsic) pathways, both of which involve the activation of a family of cysteine proteases with aspartate specificity, called caspases, as the executioners of apoptosis.[3,4] In light of urgent need for cancer therapy, development of small molecules that activate and induce apoptosis is a promising strategy for the treatment of cancer.

The pyrazole scaffold has drawn a great deal of attention due to its applications in biological and pharmacological fields regardless of scarcity in nature.[5] For example, N-substituted pyrazoles such as pirazolac and difenamizole are known as nonsteroidal anti-inflammatory drugs (NSAIDs). On the other hand, celecoxib, a selective cyclooxygenase-2 (COX-2) inhibitor, is clinically used for the therapy of osteoarthritis, rheumatoid arthritis, acute pain and so on. It has also been further examined to reduce numbers of colon and rectum polyps in patients with familial adenomatous polyposis. In addition, N-substituted pyrazoles have been also developed as inhibitors of p38, SERMs and inhibitors of aurora-A kinase potentially used as anticancer agents. Nevertheless, the abovementioned pyrazoles are mainly focused on the exploitation of N-substituted derivatives for pharmacological purposes. Until recently, several 3,5-diary-*1H*-pyrazoles were reported as inhibitors of monoamine oxidases. In continuation of our research on the development of small molecules targeting cancer cells, we attempted to introduce 3,5-diaryl-*1H*-pyrazole as a molecular scaffold with aim to examine their anticancer effect in the present study.

2. Results and Discussion

2.1 Synthesis of 3,5-diaryl-*1H*-pyrazoles 1-33

The preparation of 3,5-diaryl-*1H*-pyrazole was originally from the cyclization of 1,3-diketone and hydrazine in 1893. Although several methods have been developed, there are some tedious procedures or more reagents needed to handle with. In the beginning, we carried out the nucleophilic substitution between commerically available acetophenone and acyl chloride in the presence of strong base n-BuLi to afford 1,3-diketone. Without further purification, 1,3-diketone was underwent cyclization with hydrazine in refluxed ethanol to give 3,5-diaryl-*1H*-pyrazole. The acetophenone was initially deprotonated by n-BuLi to generate a nucleophilc enolate, followed by the nucleophilic substitution with acyl chloride to afford 1,3-diketone. Nevertheless, some side products appeared during the preparation of 1,3-diketone. The formation of side products might be attributed to the self-condensation of acetophenone. Moreover, n-butyl chloride was also found to serve as a nucleophile to attack acyl chloride that afforded 1-aryl-pentan-1-ones. Therefore, we applied a more updated synthetic method with slight modifications as reported in the literature [3]. As shown in Scheme 1, both two equivalents of acetophenone and lithium bis(trimethylsilyl)amide (LiHMDS) and one equivalent of acyl chloride were charged in the toluene. The reaction solution was evaporated *in vacuo* to obtain the crude 1,3-diketone, followed by the addition of hydrazine in refluxed ethanol to afford 3,5-diaryl-*1H*-pyrazoles. The strong base LiHMDS used in this method is more advantageous than n-BuLi thanks to the poor nucelophilicity. Consequently, we synthesized a series of 3,5-diaryl-*1H*-pyrazoles, some of which were subjected to hydrogenation or demethylation reaction to afford the corresponding products (Scheme 2).

Scheme 1

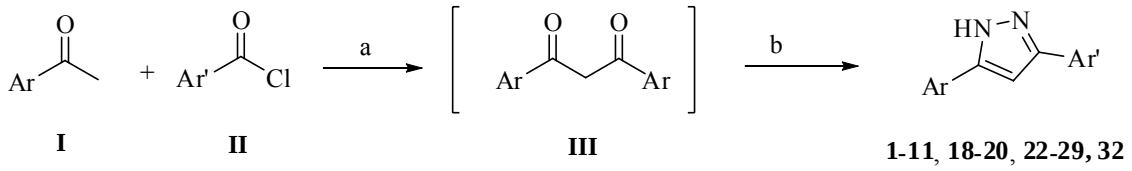

Reagents: (a) LiHMDS, toluene, 0 °C, 2h; (b) NH_2NH_2 HCl, EtOH, reflux, 16h.

Scheme 2

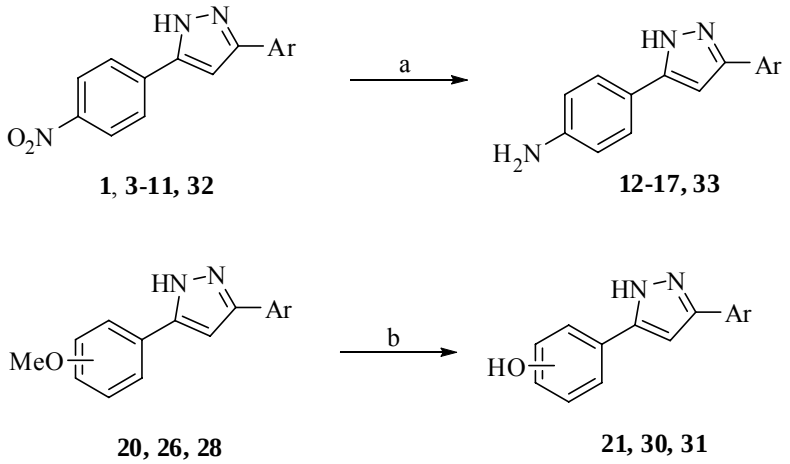

Reagents : (a) Pd/C, H_2, MeOH, r.t., 16 h; (b) BBr_3, DCM

2.2 Growth inhibition of 1-33 against four carcinoma cells

The evaluation of growth-inhibitory activity of 3,5-diaryl-*1H*-pyrazoles **1-33** was examined on a panel of human carcinoma cell lines, including OVCA (ovarian carcinoma cell), SW620 (colorectal adenocarcinoma cell), H460 (esophageal carcinoma cell) and AGS (gastric carcinoma cell). The MTT assay was employed for growth inhibition studies and the GI_{50} values are summarized in Table 1, 2 and 3. The tested compound concentration causing a 50% cell growth inhibition (GI_{50}) was determined by interpolation from dose-response curves.

As indicated in Table 1, **1-11** represent the 3,5-diaryl-*1H*-pyrazoles bearing an electron-withdrawing nitro group at 4- or 3-position on one benzene ring while various substituents on another. Among four carcinoma cell lines, OVCA and H460 cell lines seemed to be more sensitive in response to the growth inhibition with GI_{50} values between 5.8 and 28.9 μM. Compared to the mono-substituted counterparts, disubstituted **6** and **7** displayed higher activities against most cell lines. Interestingly, except for **11**, substituents at 4-position such as **6-10** showed better activity than the counterparts **1-5** against SW620 cells.

Table 1. Chemical structures and GI_{50} values of 3, 5-diarylpyrazoles **1-11**.

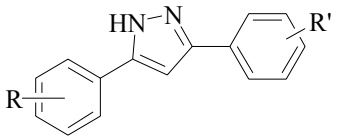

R = 4-NO_2 **1**, **3-11**
R = 3-NO_2 **2**

		GI_{50} (μM) [a]			
Entry	R'	OVCA	SW620	H460	AGS
1	hydrogen	7.2 ± 1.8	ND [b]	10.2 ± 1.9	ND
2	hydrogen	5.8 ± 0.4	ND	6.1 ± 2.6	11.4 ± 0.9
3	2-methoxy	11.7 ± 0.9	ND	20.5 ± 4.7	ND
4	3-methoxy	19.1 ± 5.1	ND	11.2 ± 2.4	ND
5	4-methoxy	27.3 ± 4.3	14.3 ± 1.8	18.3 ± 5.6	ND
6	3,4-dimethoxy	28.9 ± 5.3	26.4 ± 1.1	17.9 ± 4.8	ND
7	3,4-methylenedioxy	10.8 ± 1.8	23.5 ± 3.4	8.9 ±2.2	13.1 ± 1.3
8	4-fluoro	ND	18.1 ± 1.2	ND	18.3 ± 0.3
9	4-chloro	ND	12.2 ± 1.8	20.7 ± 6.2	24.1 ± 0.8
10	4-bromo	17.5 ± 3.2	28.6 ± 2.9	ND	14.6 ± 0.5
11	4-trifluoromethyl	ND	ND	ND	ND

[a] GI_{50} values are presented as the mean ± SEM (standard error of the mean) from four to six separated experiments.

[b] ND indicated that no appreciable growth inhibition was observed upon treatment of maximal concentration at 40 μM.

Following by the reduction of the nitro group in **1** and **3-7** to generate the corresponding the amino-containing counterparts **12-17** bearing an electron-donating amino substituent, most of which revealed no growth-inhibitory effect. Nevertheless, in comparison with the counterpart **11** (4-NO_2)**,** **17** (4-NH_2) showed an improved growth-inhibitory effect against OVCA and H460 cell lines with GI_{50} values of 18.6 and 21.5 μM, respectivity (Table 2). These findings suggest that either electron-donating or electron-withdrawing group on both sides would result in a precipitous loss in potency. Therefore, upon replacement of the amino group in **17** (4-NH_2) with a dimethylamino group in **18** (4-NMe_2), a dramatic decrease in activity was observed, suggesting that amino group with hydrogen bond-donating character plays an important role for activity.

Table 2. Chemical structures and GI_{50} values of 3, 5-diarylpyrazoles **12-25**.

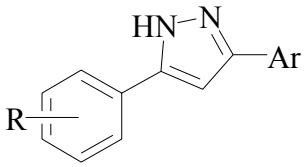

R = 4-NH_2 **12-17** R = 4-NMe_2 **18**
R = 4-OMe **19, 20**, **22-25** R = 4-OH **21**

		GI_{50} (μM)[a]			
Entry	Ar	OVCA	SW620	H460	AGS
12	phenyl	ND[b]	25.4 ± 2.4	26.7 ± 0.9	ND
13	2-methoxyphenyl	ND	21.1 ± 1.2	ND	ND
14	3-methoxyphenyl	ND	ND	ND	ND
15	4-methoxyphenyl	ND	ND	ND	ND
16	3,4-dimethoxyphenyl	ND	ND	ND	ND
17	4-trifluoromethylphenyl	18.6 ± 5.5	ND	21.5 ± 3.1	ND
18	4-trifluoromethylphenyl	ND	ND	ND	ND
19	phenyl	9.9 ± 1.9	27.2 ± 3.8	10.4 ± 3.4	11.3 ± 0.7
20	4-trifluoromethylphenyl	22.8 ± 3.5	11.2 ± 1.1	ND	14.8 ± 0.3
21	4-trifluoromethylphenyl	9.2 ± 1.0	19.6 ± 1.8	20.1 ± 2.4	9.8 ± 0.9
22	4-fluorophenyl	14.0 ± 2.7	ND	ND	ND
23	4-chlorophenyl	12.8 ± 2.9	ND	11.6 ± 4.1	ND
24	4-bromophenyl	20.7 ± 2.1	ND	27.1 ± 3.9	ND
25	2-naphthyl	17.5 ± 1.6	26.9 ± 2.3	13.2 ± 1.0	19.0 ± 0.4

[a] GI_{50} values are presented as the mean ± SEM (standard error of the mean) from four to six separated experiments.

[b] ND indicated that no appreciable growth inhibition was observed upon treatment of maximal concentration at 40 μM.

It is worthwhile to notice that **19** without substituent on one benzene exhibited activity against SK-OV-3, OVCA, SW620, H460 and AGS cell lines with GI_{50} values of 36.2, 9.9, 27.2, 10.4 and 11.3 μM, respectively, which were more active than **22-24** with substitutents on both sides. In addition to the modulations of electronic factors on the benzene, we further built a more steric demanded modification of which a phenyl group was introduced at 2-position based on the structure of compound **19**. As a result, a series of 1,1'-biphenyl analogs **26-33** were synthesized with a

dramatic increase in growth inhibition as indicated in Table 3.

Table 3. Chemical structures and GI_{50} values of 3, 5-diaryl-*1H*-pyrazoles **26-33**.

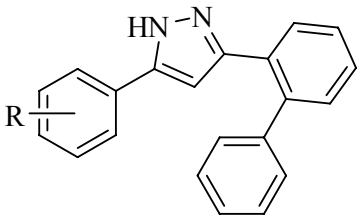

26-33

		GI_{50} (μM)[a]			
Entry	R	OVCA	SW620	H460	AGS
26	4-OMe	0.67 ± 0.1	0.89 ± 0.12	0.73 ± 0.11	0.79 ± 0.08
27	4-CF_3	2.75 ± 0.1	ND[b]	ND	6.9 ± 0.7
28	2-OMe	14.2 ± 1.1	ND	9.1 ± 2.5	ND
29	3-OMe	5.8 ± 1.3	ND	8.7 ± 1.4	7.5 ± 0.8
30	2-OH	5.8 ± 0.4	10.6 ± 0.7	4.6 ± 1.2	7.5 ± 0.5
31	4-OH	6.2 ± 0.6	25.9 ± 4.6	6.9 ± 1.5	9.2 ± 0.6
32	4-NO_2	3.4 ± 0.4	12.2 ± 1.2	2.7 ± 1.1	1.2 ± 0.1
33	4-NH_2	17.9 ± 1.1	ND	8.2 ± 1.3	8.4 ± 0.6

[a] GI_{50} values are presented as the mean ± SEM (standard error of the mean) from four to six separated experiments.

[b] ND indicated that no appreciable growth inhibition was observed upon treatment of maximal concentration at 40 μM.

As shown, **26** displayed the most potent activity among analogs against OVCA, SW620, H460 and AGS cell lines with GI_{50} values of 0.67, 0.89, 0.73 and 0.79 μM, respectively. Interestingly, as the methoxy group replaced with a hydroxyl group to generate **31**, a precipitous drop in potency against all cell lines was significantly observed. Likewise, as the nitro group in **32** was converted into the amino group-containing **33**, a significant decrease in potency was observed in all cell lines. The results suggest that a hydrogen-bond donor such as hydroxyl and amino groups at 4-position of benzene ring potentially counteract the 1,1'-biphenyl analogs for growth-inhibitory effect. On the other hand, as 4-methoxygroup was replaced with 2- or 3-methoxy group, a precipitous decreases in potency was also observed, suggesting that substituents at 4-position exhibit a favorable interaction between the receptors for growth inhibitor. On the contrary, 2-hydroxy substituted **30** showed at

least 2-fold more potent than the counterpart **28** bearing 2-methoxy group. We assume that the enhanced activity might be attributed to the intramolecular hydrogen bonding between the hydroxyl group and nitrogen atom on the pyrazole core that maintains the rigidity in structure for growth-inhibitory activity.

2.3 Induction of apoptosis by 26 and 27 through caspase-dependent pathways and inactivation of Akt

To demonstrate whether the cell growth inhibition was related to cell cycle regulation and apoptosis, **26** and **27** were selected for further mechanistic study on OVCA cells. As indicated in the flow cytometric analysis (Figure 1), OVCA cells exposed to **26** and **27** for 24hr exhibited the accumulation of sub-G1 arrest in a dose-dependent manner. As shown, the exposure of OVCA cells to **26** at 1.2, 2.5 and 5.0 μM, the substantial sub-G1 arrest was detected with 14.97 20.53 and 32.05%, respectively. Similarly, OVCA treated with **27** at 1.2, 2.5 and 5.0 μM also resulted in the increasing sub-G1 arrest with 11.43, 15.75 and 23.51%, respectively. These findings suggest that growth inhibition of OVCA cells mediated by **26** and **27** may cause DNA fragmentation and cell death.

Figure 1. Flow cytometric analysis of OVCA cells. Cells were harvested after 24 h treatment and followed by fixation, propidium iodide staining prior to the flow cytometric analysis. Sub-G1 phase indicated the DNA fragmentation and cell death. Exposure of OVCA cells to **26** at 1.2, 2.5 and 5.0 μM caused the sub-G1 phase arrest with 14.97, 20.53 and 32.05%, respectively. Similarly, OVCA cells exposed to **26** at 1.2, 2.5 and 5.0 μM caused the sub-G1 phase arrest with 11.43, 15.75 and 23.51%, respectively. (A) Untreated OVCA cells were taken as blank group; (B) cells were treated with 0.5% DMSO as the control; (C) treatment of **26** at 1.2 μM; (D) treatment of **26** at 2.5 μM; (E) treatment of **26** at 5.0 μM; (F) treatment of **27** at 1.2 μM; (G) treatment of **27** at 2.5 μM; (H) treatment of **27** at 5.0 μM.

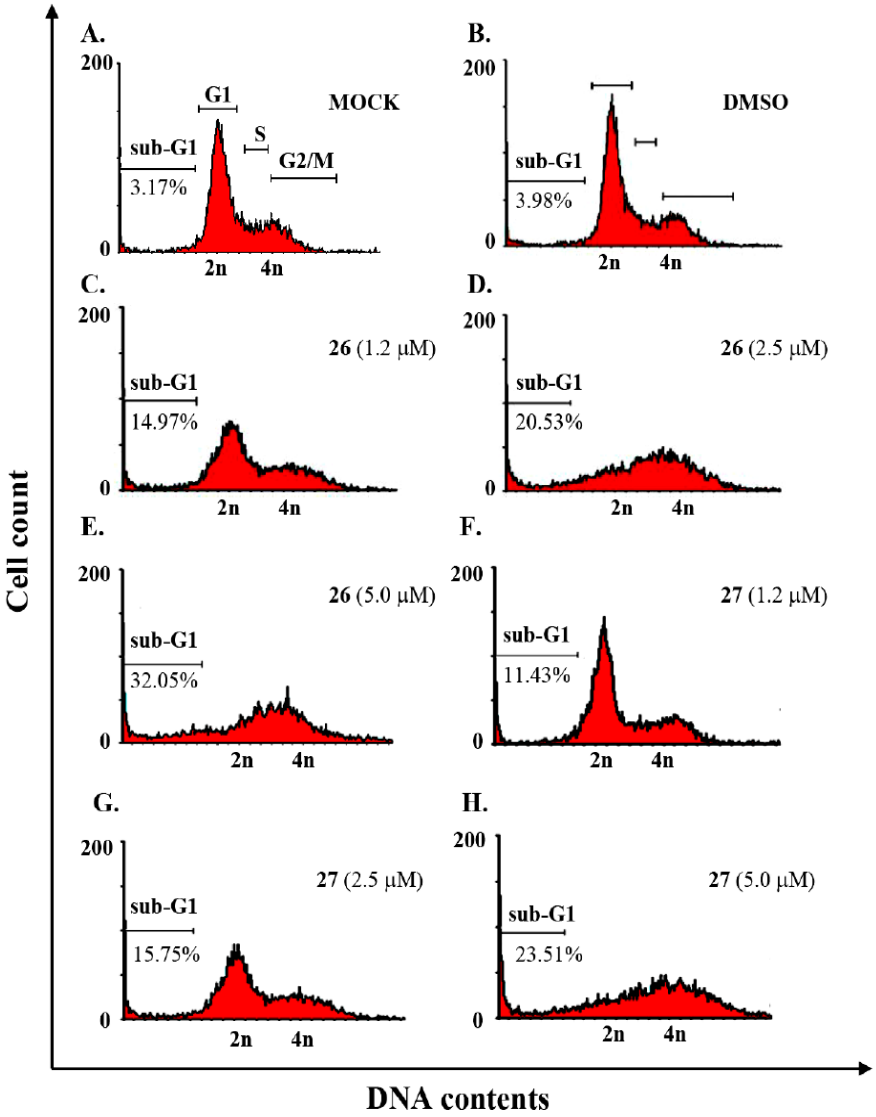

On the other hand, Western blot of cytosolic extracts prepared from **26**- and **27**-treated OVCA

cells for 16 hr revealed cleavage of the 116-kDa protein poly(ADP-ribose) polymerase (PARP) and generation of the 89-kDa fragment (Figure 2). The results were consistent with the activation of pro-apoptotic caspase-3, as shown by the increased levels of 17/19-kDa cleaved caspase-3. Moreover, the activation of the upstream caspase-9 was also monitored by the elevated levels of the cleaved 35/37-kDa caspase-9. Taken together, we conclude that the mitochondrial apoptotic pathway mediated by **26** and **27** was involved.

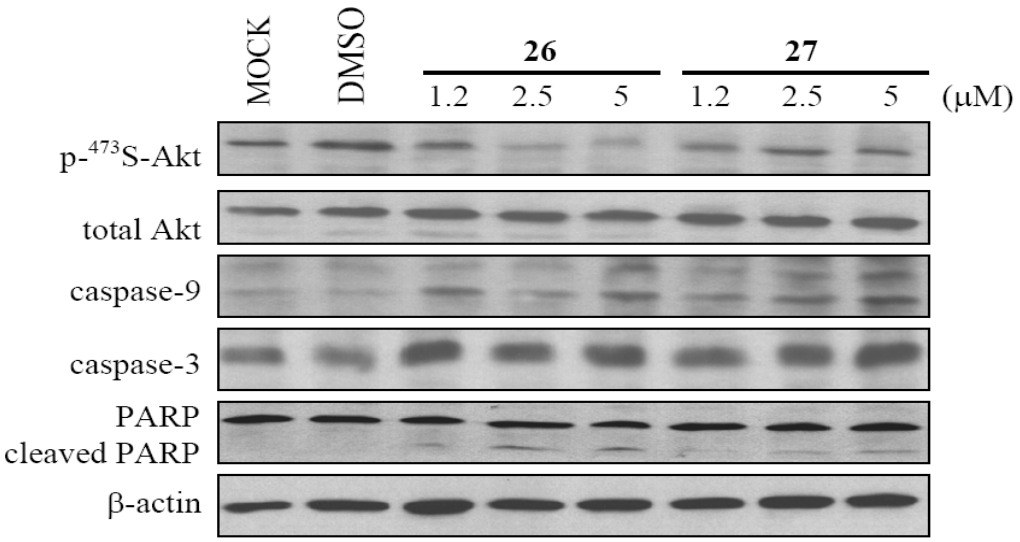

Figure 2. Induction of apoptosis in OVCA cells by **26** and **27**. Induction of poly(ADP-ribose) polymerase (PARP) cleavage by **26** and **27** at the indicated concentrations after 16h of treatment. PARP proteolysis to the apoptosis-specific 85-kDa fragment was monitored by western blotting. The appearance of a 89-kDa fragment coincided with the activation of caspase-3, as shown by the increased level of the 17/19-kDa cleaved caspase-3. The activation of the upstream caspase-9 was also observed with the increased level of the 35/37-kDa cleaved caspase-9, indicating the mitochondrial apoptotic pathway was involved. The phosphorylation status of Akt was also determined by immunoblot analysis with phosphospecific antibody. Unphosphorylated Akt, as immunostained by anti-Akt antibody, was used as internal standard for the comparison of phospho-Akt level among samples of different preparations.

Aberrant function of PI3K/Akt signaling pathway contributes to cell proliferation and survival in a variety of neoplasms including ovarian cancer. Akt is overexpressed in a substantial number of ovarian cancers, resulting in the constitutive activation of signaling pathway as indicated by phosphorylation of Akt *in vitro* and *in vivo*. In addition to the elucidation of mitochondrial apoptotic pathway, we attempted to examine the effect on the phosphorylation state of Akt due to its significance in OVCA cell survival. As indicated, the reduction of phosphorylated Akt level in response to **26** and **27** for 16hr treatment was clearly observed. Moreover, **26** exhibited more potent inhibitory effect on Akt activity than that of **27**, which is corresponding to its growth-inhibitory activity over **27** (GI_{50}, 0.67 vs. 2.75 μM). These results suggest that the induction of apoptosis by **26** and **27** in OVCA ovarian cancer cells might be, in part, attributable to the inhibition of Akt activity.

2.4 Structure-activity relationship study on OVCA cells

Structure-activity relationship analysis was further examined on OVCA cells. Comparative Molecular Field Analysis (CoMFA) was employed by software Sybyl 8.1 to characterize structure-activity relationships in this study. Our final training set model and coefficients such as non-validation R^2 and F-value were obtained by using the optimal number of components and all the data points in the training set. The cross-validated q^2 value with 0.671 and the subsequent non-validation R^2 value with 0.846 meet the criteria ($q^2 \geqq 0.5$; $R^2 \geqq 0.8$) that indicate the constructed model is internally predictive and accountable. The contributions for steric and electrostatic fields are 0.459 and 0.561, respectively. As shown in Figure 3A, all compounds were aligned to the pyrazole core as specified in stick. The steric field (in yellow/green for unfavorable/favorable contours, Figure 3B) and electrostatic field (in blue/red for positive/negative charge favorable contours, Figure 3C) projected onto **32**. In steric field model, three steric unfavorable contours near C-2', C-3', and C-4' greatly restrict the modifications around the ring A moiety. Accordingly, **1** shows a higher activity (GI_{50}, 7.2 μM) compared to **3** (GI_{50}, 11.7 μM) bearing a methoxy group on C-2' and **6** (GI_{50}, 28.9 μM) having methoxy groups on C-3' and C-4'. The steric favorable contour centering on C-6' is amenable for modifications evidenced by comparing **25** (GI_{50}, 17.5 μM) and **26** (GI_{50}, 0.67 μM) with a bulky phenyl group on C-6'. A steric

unfavorable contour is located at C-4” position on the ring B moiety, which explains the different location of a nitro group, such as C-4” in **1** and C-3” in **2**, responsible for different activities with GI_{50} values of 7.2 and 5.8 μM, respectively. In electrostatic field model (Figure 3C), the blue contour around C-2’ suggests a positively charged substituent to increase activity. As a result, **3** (GI_{50}, 11.7 μM) with a partial negatively charged methoxy oxygen atom nearby the blue contour has a lower activity compared to **1** without substituent. The mixed one blue contour and two red contours around C-4” correspondingly match a nitro group composed of a positively charged nitrogen atom and two negatively charged oxygen atoms. It interprets the dramatic discrepancy in activity between **1** (4-NO_2, GI_{50}, 7.2 μM) and **12** (4-NH_2, GI_{50}, ND) with distinct charge distribution on C-4”.

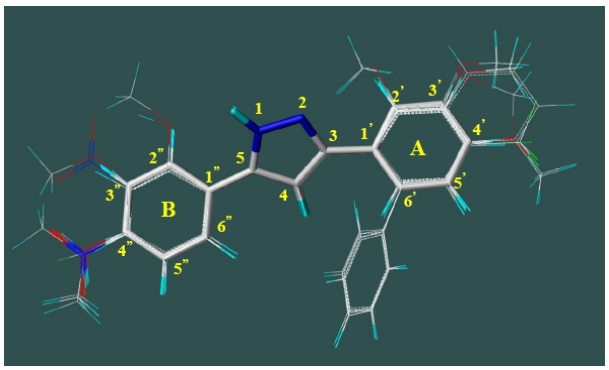

(A)

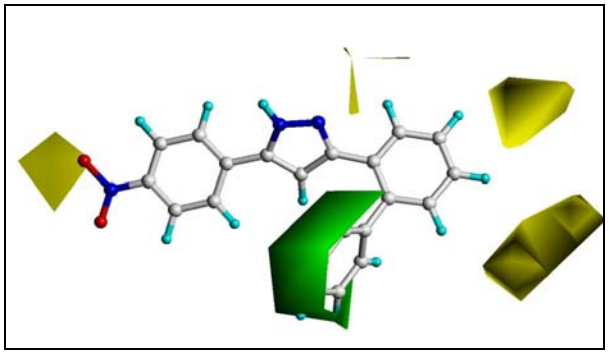

(B)

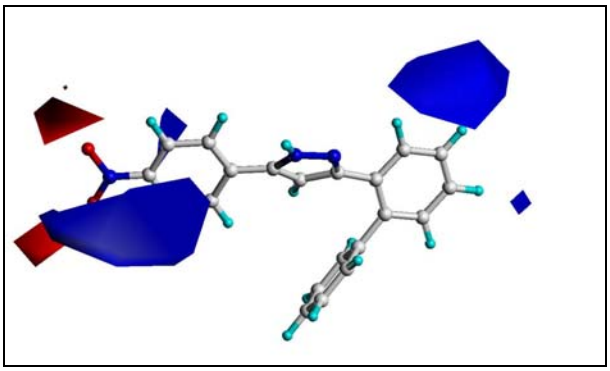

(C)

Figure 3. 3D-QSAR study on OVCA cells. Comparative Molecular Field Analysis (CoMFA) was employed by software Sybyl 8.1 to characterize structure-activity relationships. (A) Alignment of 3,5-diaryl-*1H*-pyrazoles **1-33** to the pyrazole core specified in stick. (B) Steric field projected on **32**: yellow contour indicate bulky groups decrease activity (contribution level of 80%), whereas green contours indicate bulky groups increase activity (contribution level of 20%); (C) Electrostatic field projected on **32**: red contours indicate negatively charged groups increase activity (contribution level of 20%), whereas blue contours indicate positively charged groups increase activity (contribution level of 80%).

3. **Conclusions**

In the present study, a series of 3,5-diaryl-*1H*-pyrazoles were prepared in which the condensation between acetophenone and benzoyl chloride in the presence of LiHMDS to generate 1,3-diketone, followed by the cyclization reaction by treatment of hydrazine to afford the desired products. With all tested analogs in hand, growth inhibition in a panel of four carcinoma cells. Our findings suggest that analogs bearing an electron-withdrawing group on one aromatic ring while an electron-donating group on the other exhibited better growth-inhibitory effect. In addition, as a phenyl introduced at 2-position on the aromatic ring the activity was dramatically increased. For example, **26** bearing a 1,1'-biphenyl moiety exhibited the most potent activity against OVCA, SW620, H460 and AGS cells with GI_{50} values of 0.67, 0.89, 0.73 and 0.79 μM, respectively. The mechanistic study on OVCA cells demonstrated that growth inhibition mediated by **26** and **27** was, in part, attributed to the inhibition of intracellular Akt activity, followed by the mitochondrial apoptotic pathway via the activation of caspase-9, caspase-3, cleavage of protein poly(ADP-ribose) polymerase (PARP) and DNA fragmentation. Moreover, structure-activity relationship analysis employed by Comparative Molecular Field Analysis (CoMFA) model was generated with q^2 and R^2 values of 0.671 and 0.846, respectively, suggesting its predictivity and accountability for further study.

4. Experimental

4.1. Synthesis

Chemical reagents and organic solvents were purchased from TCI, Alfa Aesar and Acros. Melting points were determined by Fargo MP-2D. Nuclear magnetic resonance spectra (^{1}H and ^{13}C NMR) were measured on a Bruker AC-300 instrument. Chemical shifts (d) are reported in ppm relative to the TMS peak. High Resolution Mass spectra (HRMS) were obtained by FAB on a Jeol JMS-700 instrument. Flash column chromatography was performed with silica gel (230–400 mesh).

4.1.1. The general experimental procedure

5-(4-nitrophenyl)-3-phenyl-1*H*-pyrazole (1)

M.p. 281 ^{o}C. ^{1}H NMR (300 MHz, DMSO-d_6) δ 7.38 (t, J = 7.3 Hz, 1H), 7.42 (s, 1H), 7.49 (dd, J = 7.6, 7.3 Hz, 2H), 7.84 (d, J = 7.6 Hz, 2H), 8.12 (d, J = 8.6 Hz, 2H), 8.31 (d, J = 8.6 Hz, 2H) ppm. ^{13}C NMR (75 MHz, DMSO-d_6) δ 101.21, 124.19, 125.18, 125.83, 128.22, 128.95, 146.43 ppm. HRMS $(M+1)^+$ calcd for $C_{15}H_{11}N_3O_2$ 266.0885; found 266.0931.

4.1.2 5-(3-nitrophenyl)-3-phenyl-1*H*-pyrazole (2)

M.p. 214 ^{o}C. ^{1}H NMR (300 MHz, DMSO-d_6) δ 7.36 (t, J = 7.3 Hz, 1H), 7.42 (s, 1H), 7.47 (dd, J = 7.5, 7.3 Hz, 2H), 7.76 (dd, J = 8.0, 7.6 Hz, 1H), 7.84 (d, J = 7.5 Hz, 2H), 8.16 (d, J = 8.0 Hz, 1H), 8.28 (d, J = 7.6 Hz, 1H), 8.66 (s, 1H), 13.61 (brs, NH) ppm. ^{13}C NMR (75 MHz, DMSO-d_6) δ 100.38, 119.20, 122.01, 125.17, 128.35, 129.02, 130.30, 131.32, 135.32, 143.95, 148.35, 149.28 ppm. HRMS $(M)^+$ calcd for $C_{15}H_{11}N_3O_2$ 265.0851; found 265.0848.

3-(2-methoxyphenyl)-5-(4-nitrophenyl)-1*H*-pyrazole (3)

M.p. 226 ^{o}C. ^{1}H NMR (300 MHz, DMSO-d_6) δ 3.92 (s, 3H), 7.05 (dd, J = 7.5, 7.2 Hz, 1H), 7.15 (d, J = 8.3 Hz, 1H), 7.34 (s, 1H), 7.36 (dd, J = 8.3, 7.2 Hz, 1H), 7.77 (d, J = 7.5 Hz, 1H), 8.11 (d, J = 8.8 Hz, 2H), 8.28 (d, J = 8.8 Hz, 2H), 13.27 (brs, NH) ppm. ^{13}C NMR (75 MHz, DMSO-d_6) δ 55.53, 103.27, 111.95, 120.72, 124.17, 125.79, 127.74, 129.70, 139.79, 146.33, 155.78 ppm. HRMS $(M)^+$ calcd for $C_{16}H_{13}N_3O_3$ 295.0957; found 295.0955.

4.1.3 3-(3-methoxyphenyl)-5-(4-nitrophenyl)-1*H*-pyrazole (4)

M.p. 233 ^{o}C. ^{1}H NMR (300 MHz, DMSO-d_6) δ 3.81 (s, 3H), 6.93 (d, J = 6.7 Hz, 1H), 7.38 (dd, J = 7.2, 6.7 Hz, 1H), 7.39 (d, J = 7.2 Hz, 1H), 7.40 (s, 1H), 7.44(s, 1H), 8.11 (d, J = 8.8 Hz, 2H), 8.31 (d, J = 8.8 Hz, 2H), 13.70 (brs, NH) ppm. ^{13}C NMR (75 MHz, DMSO-d_6) δ 55.21, 101.41, 110.60, 113.92, 117.53, 124.19, 125.82, 125.97, 130.11, 146.44, 159.72 ppm. HRMS $(M)^+$ calcd for $C_{16}H_{13}N_3O_3$ 295.0957; found 295.0959.

4.1.4 3-(4-methoxyphenyl)-5-(4-nitrophenyl)-1*H*-pyrazole (5)

M.p. 205 ^{o}C. ^{1}H NMR (300 MHz, DMSO-d_6) δ 3.79 (s, 3H), 7.04 (d, J = 8.6 Hz, 2H), 7.30 (s, 1H), 7.76 (d, J = 8.6 Hz, 2H), 8.10 (d, J = 8.8 Hz, 2H), 8.30 (d, J = 8.8 Hz, 2H), 13.54 (brs, NH) ppm. ^{13}C NMR (75 MHz, DMSO-d_6) δ 55.22, 100.09, 114.45, 124.10, 125.77, 126.61, 146.35, 159.36 ppm. HRMS $(M)^+$ calcd for $C_{16}H_{13}N_3O_3$ 295.0957; found 295.0963.

4.1.5 3-(3,4-dimethoxyphenyl)-5-(4-nitrophenyl)-1*H*-pyrazole (6)

M.p. 194 °C. ^{1}H NMR (300 MHz, DMSO-d_6) δ 3.79 (s, 3H), 3.85 (s, 3H), 7.04 (d, J = 8.2 Hz, 1H), 7.32 (s, 1H), 7.36 (d, J = 8.2 Hz, 1H), 7.43 (s, 1H), 8.10 (d, J = 8.4 Hz, 2H), 8.28 (d, J = 8.4 Hz, 2H), 13.58 (br s, NH) ppm. ^{13}C NMR (75 MHz, DMSO-d_6) δ 55.56, 55.65, 100.29, 109.11, 112.10, 117.75, 121.68, 124.11, 125.75, 140.21, 144.23, 146.34, 149.04, 149.19 ppm. HRMS $(M)^+$ calcd for $C_{17}H_{15}N_3O_4$ 325.1063; found 325.1060.

4.1.6 3-(benzo[d][1,3]dioxol-5-yl)-5-(4-nitrophenyl)-1*H*-pyrazole (7)

M.p. 249 °C. ^{1}H NMR (300 MHz, DMSO-d_6) δ 6.06 (s, 2H), 7.01 (d, J = 7.6 Hz, 1H), 7.27 (s, 1H), 7.31 (d, J = 7.6 Hz, 1H), 7.37 (s, 1H), 8.07 (d, J = 7.9 Hz, 2H), 8.23 (d, J = 7.9 Hz, 2H), 13.53 (br s, NH) ppm. ^{13}C NMR (75 MHz, DMSO-d_6) δ 100.54, 101.38, 105.66, 108.82, 119.13, 123.04, 124.14, 125.78, 140.11, 143.98, 146.41, 147.40, 147.90, 149.26 ppm. HRMS $(M)^+$ calcd for $C_{16}H_{11}N_3O_4$ 309.0750; found 309.0749.

4.1.7 3-(4-fluorophenyl)-5-(4-nitrophenyl)-1*H*-pyrazole (8)

M.p. 302 °C. ^{1}H NMR (300 MHz, DMSO-d_6) δ 7.31 (d, J = 5.2 Hz, 2H), 7.35 (s, 1H), 7.85 (s, J = 5.2 Hz, 2H), 8.09 (d, J = 8.4 Hz, 2H), 8.27 (d, J = 8.4 Hz, 2H), 13.70 (brs, NH) ppm. ^{13}C NMR (75 MHz, DMSO-d_6) δ 101.04, 115.88, 124.11, 125.81, 127.29, 143.12, 163.62 ppm. HRMS $(M)^+$ calcd for $C_{15}H_{10}FN_3O_2$ 283.0757; found 283.0761.

4.1.8 3-(4-chlorophenyl)-5-(4-nitrophenyl)-1*H*-pyrazole (9)

M.p. 280 °C. ^{1}H NMR (300 MHz, DMSO-d_6) δ 7.41 (s, 1H), 7.51 (d, J = 8.4 Hz, 2H), 7.85 (d, J = 8.4 Hz, 2H), 8.08 (d, J = 8.7 Hz, 2H), 8.28 (d, J = 8.7 Hz, 2H), 13.74 (brs, NH) ppm. ^{13}C NMR (75 MHz, DMSO-d_6) δ 101.59, 124.22, 125.86, 126.90, 128.96, 132.66, 146.48 ppm. HRMS $(M)^+$ calcd for $C_{15}H_{10}ClN_3O_2$ 299.0462; found 299.0459.

4.1.9 3-(4-bromophenyl)-5-(4-nitrophenyl)-1*H*-pyrazole (10)

M.p. 258 °C. ^{1}H NMR (300 MHz, DMSO-d_6) δ 7.36 (s, 1H), 7.62 (d, J = 8.5 Hz, 2H), 7.77 (d, J = 8.5 Hz, 2H), 8.06 (d, J = 8.7 Hz, 2H), 8.25 (d, J = 8.7 Hz, 2H), 13.80 (brs, NH) ppm. ^{13}C NMR (75 MHz, DMSO-d_6) δ 101.54, 121.21, 124.17, 125.87, 127.20, 131.83, 146.45 ppm. HRMS $(M)^+$ calcd for $C_{15}H_{10}ClN_3O_2$ 299.0462; found 299.0459.

4.1.10 5-(4-nitrophenyl)-3-(4-(trifluoromethyl)phenyl)-1*H*-pyrazole (11)

M.p. 244 ^{o}C. ^{1}H NMR (300 MHz, DMSO-d_6) δ 7.58 (s, 1H), 7.84 (d, J = 8.3 Hz, 2H), 8.06 (d, J = 8.3 Hz, 2H), 8.12 (d, J = 8.8 Hz, 2H), 8.33 (d, J = 8.8 Hz, 2H), 13.93 (brs, NH) ppm. ^{13}C NMR (75 MHz, DMSO-d_6) δ 102.45, 124.29, 125.72, 125.93, 128.19, 146.61 ppm. HRMS $(M)^+$ calcd for $C_{16}H_{10}F_3N_3O_2$ 333.0725; found 333.0730.

4.1.11 4-(3-phenyl-1H-pyrazol-5-yl)aniline (12)

M.p. 163 ^{o}C. ^{1}H NMR (300 MHz, DMSO-d_6) δ 5.58 (brs, NH_2), 6.64 (d, J = 8.4 Hz, 2H), 6.90 (s, 1H), 7.29 (t, J = 7.3 Hz, 1H), 7.34 (dd, J = 7.7, 7.3 Hz, 2H), 7.52 (d, J = 8.4 Hz, 2H), 7.81 (d, J = 7.7 Hz, 2H), 12.83 (brs, NH) ppm. ^{13}C NMR (75 MHz, DMSO-d_6) δ 97.70, 111.67, 114.21, 125.02, 126.15, 127.42, 127.78, 128.67, 128.82, 148.08 ppm. HRMS $(M)^+$ calcd for $C_{15}H_{13}N_3$ 235.1109; found 235.1113.

4.1.12 4-(3-(2-methoxyphenyl)-1H-pyrazol-5-yl)aniline (13)

M.p. 158 ^{o}C. ^{1}H NMR (300 MHz, DMSO-d_6) δ 3.89 (s, 3H), 7.00 (d, J = 8.3 Hz, 2H), 7.01 (dd, J = 7.8, 7.3 Hz, 1H), 7.02 (s, 1H), 7.11 (d, J = 8.3 Hz, 1H), 7.31 (dd, J = 8.3, 7.8 Hz, 1H), 7.70 (d, J = 8.3 Hz, 2H), 7.79 (d, J = 7.3 Hz, 1H) ppm. ^{13}C NMR (75 MHz, DMSO-d_6) δ 55.48, 101.41, 111.89, 114.15, 118.30, 120.62, 126.15, 127.66, 129.13, 155.87 ppm. HRMS $(M)^+$ calcd for $C_{16}H_{15}N_3O$ 265.1215; found 265.1218.

4.1.13 4-(3-(3-methoxyphenyl)-1*H*-pyrazol-5-yl)aniline (14)

M.p. 86 ^{o}C. ^{1}H NMR (300 MHz, $CDCl_3$) δ 3.64 (s, 3H), 5.80 (brs, NH_2), 6.57 (d, J = 8.3 Hz, 2H), 6.63 (s, 1H), 6.81 (d, J = 7.7 Hz, 1H), 7.26 (dd, J = 7.7, 4.8 Hz, 1H), 7.27 (s, 1H), 7.27 (d, J = 4.8 Hz, 1H), 7.42 (d, J = 8.3 Hz, 2H), 12.82 (brs, NH) ppm. ^{13}C NMR (75 MHz, $CDCl_3$) δ 55.27, 99.11, 110.67, 114.24, 115.43, 118.36, 121.41, 126.96, 129.85, 133.55, 146.68, 147.94, 149.72, 160.01 ppm. HRMS $(M)^+$ calcd for $C_{16}H_{15}N_3O$ 265.1215; found 265.1217.

4.1.14 4-(3-(4-methoxyphenyl)-1*H*-pyrazol-5-yl)aniline (15)

M.p. 173 ^{o}C. ^{1}H NMR (300 MHz, DMSO-d_6) δ 3.77 (s, 3H), 5.25 (brs, NH_2), 6.61 (d, J = 8.5 Hz, 2

H), 6.78 (s, 1H), 6.97 (d, J = 8.7 Hz, 2H), 7.46 (d, J = 8.5 Hz, 2H), 7.72 (d, J = 8.7 Hz, 2H), 12.84 (brs, NH) ppm. ^{13}C NMR (75 MHz, DMSO-d_6) δ 55.14, 97.02, 113.88, 114.09, 126.12, 126.35, 148.61, 158.75 ppm. HRMS $(M)^+$ calcd for $C_{16}H_{15}N_3O$ 265.1215; found 265.1218.

4.1.15 4-(3-(3,4-dimethoxyphenyl)-1*H*-pyrazol-5-yl)aniline (16)

M.p. 105 ^{o}C. ^{1}H NMR (300 MHz, DMSO-d_6) δ 3.77 (s, 3H), 3.80 (s, 3H), 5.27 (brs, NH_2), 6.60 (d, J = 8.3 Hz, 2H), 6.84 (s, 1H), 6.98 (d, J = 8.4 Hz, 1H), 7.32 (d, J = 8.4 Hz, 1H), 7.38 (s, 1H), 7.46 (d, J = 8.3 Hz, 2H), 12.82 (brs, NH) ppm. ^{13}C NMR (75 MHz, DMSO-d_6) δ 55.54, 97.30, 108.93, 112.01, 113.88, 117.52, 126.13, 148.41, 148.58, 148.90 ppm. HRMS $(M)^+$ calcd for $C_{17}H_{17}N_3O_2$ 295.1321; found 295.1325.

4.1.16 4-(3-(4-(trifluoromethyl)phenyl)-1*H*-pyrazol-5-yl)aniline (17)

M.p. 266 ^{o}C. ^{1}H NMR (300 MHz, DMSO-d_6) δ 5.33 (brs, NH_2), 6.61 (d, J = 8.4 Hz, 2H), 7.02 (s, 1 H), 7.46 (d, J = 8.4 Hz, 2H), 7.76 (d, J = 8.2 Hz, 2H), 8.02 (d, J = 8.2 Hz, 2H), 13.18 (brs, NH) ppm. ^{13}C NMR (75 MHz, DMSO-d_6) δ 98.27, 113.92, 122.61, 125.48, 126.27, 127.52, 148.98 ppm. HRMS $(M)^+$ calcd for $C_{16}H_{12}F_3N_3$ 303.0983; found 303.0984.

4.1.17 N,N-dimethyl-4-(3-(4-(trifluoromethyl)phenyl)-1*H*-pyrazol-5-yl)aniline (18)

M.p. 248 ^{o}C. ^{1}H NMR (300 MHz, DMSO-d_6) δ 2.92 (s, 6H), 6.77 (d, J = 8.2 Hz, 2H), 7.07 (s, 1H), 7.63 (d, J = 8.2 Hz, 2H), 7.75 (d, J = 7.8 Hz, 2H), 8.04 (d, J = 7.8 Hz, 2H), 13.26 (brs, NH) ppm. ^{13}C NMR (75 MHz, DMSO-d_6) δ 39.97, 98.52, 112.32, 116.94, 122.67, 125.60, 126.19, 127.62, 129.87, 137.94, 144.65, 149.76, 150.25 ppm.HRMS $(M)^+$ calcd for $C_{18}H_{16}F_3N_3$ 331.1296; found 331.1299.

4.1.18 5-(4-methoxyphenyl)-3-phenyl-1*H*-pyrazole (19)

M.p. 178 ^{o}C. ^{1}H NMR (300 MHz, DMSO-d_6) δ 3.77 (s, 3H), 7.00 (d, J = 8.0 Hz, 2H), 7.06 (s, 1H), 7.32 (t, J = 7.0, 1H), 7.43 (dd, J = 7.2, 7.0, 2H), 7.77 (d, J = 8.0 Hz, 2H), 7.84 (d, J = 7.2, 2H), 13.30 (brs, NH) ppm. ^{13}C NMR (75 MHz, DMSO-d_6) δ 55.13, 98.80, 114.21, 125.08, 126.48, 127.62, 128.73, 158.99 ppm. HRMS $(M)^+$ calcd for $C_{16}H_{14}N_2O$ 250.1106; found 250.1101.

4.1.19 3-(4-methoxyphenyl)-5-(4-(trifluoromethyl)phenyl)-1H-pyrazole (20)

M.p. 221 °C. ^{1}H NMR (300 MHz, DMSO-d_6) δ 3.78 (s, 3H), 7.03 (d, J = 8.6 Hz, 2H), 7.20 (s, 1H), 7.75 (d, J = 8.6 Hz, 2H), 7.77 (d, J = 8.0 Hz, 2H), 8.04 (d, J = 8.0 Hz, 2H), 13.43 (brs, NH) ppm. ^{13}C NMR (75 MHz, DMSO-d_6) δ 55.18, 99.43, 114.03, 114.41, 121.70, 125.51, 125.88, 126.55, 127.51, 137.66, 143.69, 149.74, 159.27 ppm. HRMS $(M)^+$ calcd for $C_{17}H_{13}F_3N_2O$ 318.0980; found 318.0987.

4.1.20 4-(3-(4-(trifluoromethyl)phenyl)-1*H*-pyrazol-5-yl)phenol (21)

M.p. 207 °C. ^{1}H NMR (300 MHz, DMSO-d_6) δ 6.84 (d, J = 8.5 Hz, 2H), 7.13 (s, 1H), 7.62 (d, J = 8.5 Hz, 2H), 7.78 (d, J = 8.2 Hz, 2H), 8.03 (d, J = 8.2 Hz, 2H), 9.65 (brs, OH), 13.30 (brs, NH) ppm. ^{13}C NMR (75 MHz, DMSO-d_6) δ 99.28, 115.65, 125.51, 125.61, 125.66, 126.65, 126.59, 157.53 ppm. HRMS $(M)^+$ calcd for $C_{16}H_{11}F_3N_2O$ 304.0823; found 304.0825.

4.1.21 3-(4-fluorophenyl)-5-(4-methoxyphenyl)-1*H*-pyrazole (22)

M.p. 203 °C. ^{1}H NMR (300 MHz, DMSO-d_6) δ 3.78 (s, 3H), 7.01 (d, J = 8.4 Hz, 2H), 7.04 (s, 1H), 7.26 (dd, J = 7.6, 2.1 Hz, 2H), 7.74 (d, J = 8.4 Hz, 2H), 7.85 (dd, J = 7.6, 2.1 Hz, 2H), 13.22 (br s, NH) ppm. ^{13}C NMR (75 MHz, DMSO-d_6) δ 55.14, 98.71, 114.31, 121.98, 126.48, 126.99, 127.09, 159.10 ppm. HRMS $(M)^+$ calcd for $C_{16}H_{13}FN_2O$ 268.1012; found 268.1016.

4.1.22 3-(4-chlorophenyl)-5-(4-methoxyphenyl)-1*H*-pyrazole (23)

M.p. 221 °C. ^{1}H NMR (300 MHz, DMSO-d_6) δ 3.78 (s, 3H), 7.01 (d, J = 7.9 Hz, 2H), 7.09 (s, 1H), 7.49 (d, J = 7.2 Hz, 2H), 7.73 (d, J = 7.9 Hz, 2H), 7.84 (d, J = 7.2 Hz, 2H), 13.26 (brs, NH) ppm. ^{13}C NMR (75 MHz, DMSO-d_6) δ 55.33, 99.11, 114.47, 121.96, 126.68, 126.92, 128.86, 159.27 ppm. HRMS $(M)^+$ calcd for $C_{16}H_{13}ClN_2O$ 284.0716; found 284.0713.

4.1.23 3-(4-bromophenyl)-5-(4-methoxyphenyl)-1*H*-pyrazole (24)

M.p. 223 °C. ^{1}H NMR (300 MHz, DMSO-d_6) δ 3.78 (s, 3H), 7.01 (d, J = 8.7 Hz, 2H), 7.08 (s, 1H), 7.61 (d, J = 8.4 Hz, 2H), 7.74 (d, J = 8.7 Hz, 2H), 7.78 (d, J = 8.4 Hz, 2H), 13.29 (brs, NH) ppm. ^{13}C NMR (75 MHz, DMSO-d_6) δ 55.17, 99.02, 114.29, 120.54, 126.49, 127.04, 131.64, 159.10 ppm. HRMS $(M)^+$ calcd for $C_{16}H_{13}BrN_2O$ 328.0211; found 328.0208.

4.1.24 3-(4-methoxyphenyl)-5-(naphthalen-2-yl)-1*H*-pyrazole (25)

M.p. 266 °C. ^{1}H NMR (300 MHz, DMSO-d_6) δ 3.80 (s, 3H), 7.03 (d, J = 8.4 Hz, 2H), 7.22 (s, 1H),

7.51 (d, J = 5.9 Hz, 1H), 7.55 (d, J = 5.9 Hz, 1H), 7.78 (d, J = 8.4 Hz, 2H), 7.92 (d, J = 7.3 Hz, 2H), 7.97 (d, J = 7.3 Hz, 2H), 8.35 (s, 1H), 13.30 (brs, NH) ppm. ^{13}C NMR (75 MHz, DMSO-d_6) δ 55.17, 99.04, 114.41, 123.33, 125.73, 126.49, 127.63, 127.91, 132.45, 133.20, 143.47, 151.12, 159.17 ppm. HRMS $(M)^+$ calcd for $C_{20}H_{16}N_2O$ 300.1263; found 300.1264.

4.1.25 3-(biphenyl-2-yl)-5-(4-methoxyphenyl)-1*H*-pyrazole (26)

M.p. 159 ^{o}C. ^{1}H NMR (300 MHz, DMSO-d_6) δ 3.74 (s, 3H), 5.89 (s, 1H), 6.92 (d, J = 8.4 Hz, 2H), 7.21-7.24 (m, 2H), 7.30-7.35 (m, 4H), 7.45(d, J = 8.4 Hz, 2H), 7.45(m, 2H), 7.68 (s, 1H), 12.80, 13.07 (brs, NH) ppm. ^{13}C NMR (75 MHz, DMSO-d_6) δ 55.09, 101.39, 114.18, 126.18, 126.94, 127.46, 128.01, 129.08, 129.17, 130.38, 140.30, 158.84 ppm. HRMS $(M)^+$ calcd for $C_{22}H_{18}N_2O$ 326.1419; found 326.1425.

4.1.26 3-(biphenyl-2-yl)-5-(4-(trifluoromethyl)phenyl)-1*H*-pyrazole (27)

M.p. 170 ^{o}C. ^{1}H NMR (300 MHz, DMSO-d_6) δ 6.19 (s, 1H), 7.20-7.24 (m, 2H), 7.31-7.36 (m, 3H), 7.37(m, 1H), 7.40 (m, 2H), 7.64 (s, 1H), 7.72 (d, J = 7.8 Hz, 2H), 7.79 (d, J = 7.8 Hz, 2H), 13.29 (brs, NH) ppm. ^{13}C NMR (75 MHz, DMSO-d_6) δ 103.22, 125.35, 125.58, 125.99, 126.85, 127.18, 127.43, 127.64, 128.84, 129.00, 129.43, 130.51, 137.51, 140.50, 140.57, 143.14, 148.74 ppm. HRMS $(M)^+$ calcd for $C_{20}H_{16}N_2O$ 364.1187; found 364.1197.

4.1.27 3-(biphenyl-2-yl)-5-(2-methoxyphenyl)-1*H*-pyrazole (28)

M.p. 122 ^{o}C. ^{1}H NMR (300 MHz, DMSO-d_6) δ 3.72 (s, 3H), 6.00 (s, 1H), 6.94 (dd, J = 7.4, 7.3 Hz, 1H), 7.03 (d, J = 8.2 Hz, 1H), 7.22 (dd, J = 8.2, 7.3 Hz, 1H), 7.22-7.25 (m, 2H), 7.34 (m, 4H), 7.42 (d, J = 7.4 Hz, 1H), 7.42 (m, 2H), 7.78 (s, 1H), 12.93 (brs, NH) ppm. ^{13}C NMR (75 MHz, DMSO-d_6) δ 55.14, 105.13, 111.88, 117.78, 120.57, 126.80, 127.04, 127.41, 128.03, 128.50, 129.12, 130.37, 132.63, 138.60, 140.17, 141.82, 150.21, 155.41 ppm. HRMS $(M)^+$ calcd for $C_{22}H_{18}N_2O$ 326.1419; found 326.1424.

4.1.28 3-(biphenyl-2-yl)-5-(3-methoxyphenyl)-1*H*-pyrazole (29)

M.p. 63 ^{o}C. ^{1}H NMR (300 MHz, DMSO-d_6) δ 3.75 (s, 3H), 6.00 (s, 1H), 6.84 (d, J = 7.2 Hz, 1H), 7.15 (s, 1H), 7.15 (d, J = 6.8 Hz, 1H), 7.21-7.27 (m, 2H), 7.24 (dd, J = 7.2, 6.8 Hz, 1H), 7.30-7.37 (m, 4H), 7.46 (m, 2H), 7.69 (s, 1H), 12.93, 13.25 (brs, NH) ppm. ^{13}C NMR (75 MHz, DMSO-d_6) δ

55.04, 102.77, 110.32, 113.07, 117.30, 126.98, 127.50, 128.05, 129.09, 129.22, 129.88, 130.39, 140.37, 159.55 ppm. HRMS $(M)^+$ calcd for $C_{22}H_{18}N_2O$ 326.1419; found 326.1421.

4.1.29 2-(3-(biphenyl-2-yl)-1*H*-pyrazol-5-yl)phenol (30)

M.p. 135 ^oC. ^1H NMR (300 MHz, DMSO-d_6) δ 6.28 (s, 1H), 6.81 (dd, J = 7.4, 7.3 Hz, 1H), 6.89 (d, J = 8.0 Hz, 1H), 7.12 (dd, J = 8.0, 7.4 Hz, 1H), 7.22-7.24 (m, 2H), 7.31-7.33 (m, 3H), 7.42-7.48 (m, 3H), 7.46 (d, J = 7.3 Hz, 1H), 7.66 (s, 1H), 10.83 (brs, OH), 13.21 (brs, NH) ppm. ^{13}C NMR (75 MHz, DMSO-d_6) δ 102.96, 116.42, 116.98, 119.27, 126.59, 127.20, 127.66, 128.18, 128.82, 129.07, 129.65, 130.56, 140.71, 142.68, 150.29, 155.21 ppm. HRMS $(M)^+$ calcd for $C_{21}H_{16}N_2O$ 312.1263; found 312.1260.

4.1.30 4-(3-(biphenyl-2-yl)-1*H*-pyrazol-5-yl)phenol (31)

M.p. 119 ^oC. ^1H NMR (300 MHz, DMSO-d_6) δ 5.84 (s, 1H), 6.74 (d, J = 8.3 Hz, 2H), 7.21-7.23 (m, 2H), 7.27-7.36 (m, 3H), 7.34 (d, J = 8.3 Hz, 2H), 7.41-7.45 (m, 3H), 7.69 (s, 1H), 9.59 (brs, OH), 12.75, 13.00 (brs, NH) ppm. ^{13}C NMR (75 MHz, DMSO-d_6) δ 101.50, 115.52, 126.27, 126.93, 127.45, 128.01, 129.09, 129.18, 130.38, 140.27, 157.14 ppm. HRMS $(M)^+$ calcd for $C_{21}H_{16}N_2O$ 312.1263; found 312.1264.

4.1.31 3-(biphenyl-2-yl)-5-(4-nitrophenyl)-1*H*-pyrazole (32)

M.p. 213 ^oC. ^1H NMR (300 MHz, DMSO-d_6) δ 6.31 (s, 1H), 7.20-7.24 (m, 2H), 7.31-7.36 (m, 3H), 7.44(m, 1H), 7.50-7.52 (m, 2H), 7.60 (s, 1H), 7.87 (d, J = 8.7 Hz, 2H), 8.22 (d, J = 8.7 Hz, 2H), 13.29 (brs, NH) ppm. ^{13}C NMR (75 MHz, DMSO-d_6) δ 103.84, 124.11, 125.59, 125.98, 127.20, 127.64, 128.14, 128.99, 129.54, 130.51, 140.00, 140.38, 140.60, 143.45, 146.28, 148.24 ppm. HRMS $(M)^+$ calcd for $C_{21}H_{15}N_3O_2$ 341.1164; found 341.1165.

4.1.32 4-(3-(biphenyl-2-yl)-1*H*-pyrazol-5-yl)aniline (33)

M.p. 93 ^oC. ^1H NMR (300 MHz, DMSO-d_6) δ 5.22 (brs, NH_2), 5.74(s, 1H), 6.52 (d, J = 8.4 Hz, 2H), 7.19-7.24 (m, 2H), 7.24 (d, J = 8.4 Hz, 2H), 7.27-7.33 (m, 4H), 7.38-7.43 (m, 2H), 7.70 (s, 1H), 12.81 (brs, NH) ppm. ^{13}C NMR (75 MHz, DMSO-d_6) δ 100.70, 113.81, 125.86, 126.84, 127.37, 127.66, 127.96, 129.09, 130.34, 140.19, 141.55, 148.52 ppm. HRMS $(M)^+$ calcd for $C_{21}H_{17}N_3$ 311.1422; found 311.1418.

4.2 Cell culture

Cancer cells were purchased from Bioresource Collection and Research Center in Taiwan. Each cell line was maintained in the standard medium and grown as a monolayer in Dulbecco's Modified Eagle Medium (DMEM) containing 10% fetal bovine serum, 2 mM glutamine, 100 units/ml penicillin, and 100 g/ml streptomycin. Cultures were maintained at 37°C with 5% CO_2 in a humidified atmosphere.

4.3 MTT assay for cell viability

Cells were plated in 96-well microtiter plates at a density of 5 x 10^3/well and incubated for 24 h. After that, cells were treated with vehicle alone (control) or compounds (drugs were dissolved in DMSO previously) at the concentrations indicated. Treated cells were further incubated for 48 h. Cell survival is expressed as percentage of control cell growth. The 3-[4,5-dimethylthiazol-2-yl]-2,5-diphenyltetrazolium bromide (MTT, 2 mg/mL) dye reduction assay in 96-well microplates was used. The assay is dependent on the reduction of MTT by mitochondrial dehydrogenases of viable cell to a blue formazan product, which come be measured spectrophotometrically. Tumor cells were incubated in each well with serial dilutions of the tested compounds. After 2 days of incubation (37 ^{o}C, 5% CO_2 in a humid atmosphere) 100 μL of MTT (2 mg/mL in PBS) was added to each well and the plate was incubated for a further 2h (37°C). The resulting formazan was dissolved in 100 μL DMSO and read at 570 nm. The percentage of growth inhibition was calculated by the following equation: percentage growth inhibition = (1 x At/Ac) x 100, where At and Ac represent the absorbance in treated and control cultures, respectively. The drug concentration causing a 50% cell growth inhibition (GI_{50}) was determined by interpolation from dose-response curves. All determinations were carried out in four to six separated experiments.

4.4 Determination of apoptosis by flow cytometry

Apoptosis and cell cycle profile were assessed by DNA fluorescence flow cytometry. OVCA cells treated with 0.5% DMSO or tested compounds at indicated concentrations for 24h were harvested, rinsed in PBS, resuspended and fixed in 80% ethanol, and stored at -20 ^{o}C in fixation buffer until

ready for analysis. Then the pellets were suspended in 1 ml of fluorochromic solution (0.08 mg/mL PI (propidium iodide), 0.1% TritonX-100 and 0.2 mg/ml RNase A in 1x PBS) at room temperature in the dark for 30 min. The DNA content was analyzed by FACScan flow cytometer (Becton Dickinson, Mountain View, CA) and CELLQUEST software (Becton Dickinson). The population of apoptotic nuclei (subdiploid DNA peak in the DNA fluorescence histogram) was expressed as the percentage in the entire population.

4.5 Protein extraction and Western blotting

After the treatment of cells with vehicle (1% DMSO), **26** and **27** for indicated time treatment, the cells were washed twice with PBS and reaction was terminated by the addition of 100 μL lysis buffer. For Western blot analysis, the amount of proteins (50 μg) were separated by electrophoresis in a 15% SDS–PAGE and transferred to a nitrocellulose membrane. After an overnight incubation at 4 ^{o}C in TBST/5% non-fat milk, the membrane was washed with TBST three times and immuno-reacted with the monocolonal primary antibodies, anti-beta-actin (1:1000), anti-poly-ADP-ribose polymerase(PARP) (1:500), anti-cleaved caspase-3 (1:1000), anti-cleaved caspase-9 (1:1000), anti-phospho-Ser-473-Akt (1:1000), anti-Akt (1:1000) from Cell Signaling Technology (Beverly, MA) were used. After four washings with TBST, the anti-mouse or anti-rabbit IgG (dilute1:10,000) was applied to the membranes for 1 h at room temperature. The membranes were washed with TBST for 1 h and the detection of signal was performed with an enhanced chemiluminescence (ECL) detection reagents.

4.6 CoMFA 3D-QSAR analysis

CoMFA (Comparative Molecular Field Analysis) was carried out by software Sybyl 8.1 (Tripos International, St. Louis, Missouri, USA). MMFF94 charge assignment and force field were applied to prepare compound structures. The geometries were minimized by Powell algorithm to an energy convergence criterion of 0.01 kcal/mol Å, within 100,000 iterations. Each compound in its energetically minimized geometry was aligned. Two CoMFA descriptors including steric (Lennard-Jones 6-12 potential) and electrostatic (Coulombic potential) field energies were calculated with a sp^3 carbon atom carrying +1.0 charge to serve as a probe atom using Sybyl default

parameters. The optimal number of components (ONC = 2) was recommended after a leave-one-out cross-validated run. The final training set model and coefficients such as non-validation R^2 and F-value were obtained by using the optimal number of components and all the data points in the training set. The cross-validated $q^2 = 0.671$ and the subsequent non-validation $R^2 = 0.846$ meet the criteria $q^2 \geqq 0.5$ and $R^2 \geqq 0.8$. The contributions for steric and electrostatic fields are 0.459 and 0.561, respectively.

Acknowledgements

Financial support from the National Science Council to A. Y. Shaw is gratefully acknowledged.

References

1. Wyllie, A. H.; Kerr, J. F.; Currie, A. R. *Int. Rev. Cytol.* **1980**, *68*, 251.
2. Thompson, C. *Science* **1995**, *267*, 1456.
3. Alnemri, E. S.; Livingston, D. J.; Nicholson, D. W.; Salvesen, G.; Thornberry, N. A.; Wong, W. W.; Yuan, J. *Cell* **1996**, *87*, 171.
4. Thornberry, N.; Lazebnik, Y. *Science* 1998, *281*, 1312.
5. Parameswaran, P. S.; Naik, C. G.; Hegde, V. R. *J. Nat. Prod.* **1997**, *60*, 802.